

AN R-PROCESS KILONOVA ASSOCIATED WITH THE SHORT-HARD GRB 130603B

E. BERGER¹, W. FONG¹, AND R. CHORNOCK¹

Draft version August 6, 2013

ABSTRACT

We present ground-based optical and *Hubble Space Telescope* optical and near-IR observations of the short-hard GRB 130603B at $z = 0.356$, which demonstrate the presence of excess near-IR emission matching the expected brightness and color of an r-process powered transient (a “kilonova”). The early afterglow fades rapidly with $\alpha \lesssim -2.6$ at $t \approx 8 - 32$ hr post-burst and has a spectral index of $\beta \approx -1.5$ ($F_\nu \propto t^\alpha \nu^\beta$), leading to an expected near-IR brightness at the time of the first *HST* observation of $m_{F160W}(t = 9.4 \text{ d}) \gtrsim 29.3$ AB mag. Instead, the detected source has $m_{F160W} = 25.8 \pm 0.2$ AB mag, corresponding to a rest-frame absolute magnitude of $M_J \approx -15.2$ mag. The upper limit in the *HST* optical observations is $m_{F606W} \gtrsim 27.7$ AB mag (3σ), indicating an unusually red color of $V - H \gtrsim 1.9$ mag. Comparing the observed near-IR luminosity to theoretical models of kilonovae produced by ejecta from the merger of an NS-NS or NS-BH binary, we infer an ejecta mass of $M_{\text{ej}} \approx 0.03 - 0.08 M_\odot$ for $v_{\text{ej}} \approx 0.1 - 0.3c$. The inferred mass matches the expectations from numerical merger simulations. The presence of a kilonova provides the strongest evidence to date that short GRBs are produced by compact object mergers, and provides initial insight on the ejected mass and the primary role that compact object merger may play in the r-process. Equally important, it demonstrates that gravitational wave sources detected by Advanced LIGO/Virgo will be accompanied by optical/near-IR counterparts with unusually red colors, detectable by existing and upcoming large wide-field facilities (e.g., Pan-STARRS, DECam, Subaru, LSST).

Subject headings: gamma rays: bursts

1. INTRODUCTION

Over the past decade there has been growing circumstantial evidence linking short-duration gamma-ray bursts (GRBs) with the coalescence of compact object binaries (NS-NS and/or NS-BH; Eichler et al. 1989; Paczynski 1991; Narayan et al. 1992; Berger 2011). This evidence includes the location of some short GRBs in elliptical galaxies (Berger et al. 2005; Gehrels et al. 2005; Bloom et al. 2006; Fong et al. 2011, 2013); the absence of associated supernovae (Hjorth et al. 2005a,b; Soderberg et al. 2006; Kocevski et al. 2010); the distribution of explosion site offsets relative to the host galaxies, extending to a distance of ~ 100 kpc and matching population synthesis predictions for compact object binaries (Berger 2010; Fong et al. 2010; Fong & Begler 2013); and the lack of spatial correlation between short GRB locations and the underlying distribution of star formation or stellar mass in their hosts (Fong et al. 2010; Fong & Begler 2013). The combination of these properties clearly points to the binary merger model, but we currently lack a direct signature such as the coincident detections of gravitational waves.

Another expected signature of the merger model is an optical/infrared transient powered by r-process radioactive elements produced by the ejection of neutron-rich matter during the merger, a so-called kilonova (e.g., Li & Paczyński 1998; Metzger et al. 2010; Barnes & Kasen 2013). Recent simulations suggest an ejected mass of $\sim (0.5 - 5) \times 10^{-2} M_\odot$ (depending on the mass ratio of the binary constituents) with a velocity of $\sim 0.1 - 0.3c$ (e.g., Goriely et al. 2011; Piran et al. 2013). In addition, initial calculations by Barnes & Kasen (2013), now confirmed by others (Rosswog et al. 2013; Tanaka & Hotokezaka 2011), indicate that due to the large opacity of r-process elements such a transient is expected to peak in the near-IR with a timescale of ~ 1 week and an ab-

solute magnitude of only $M_J \sim -15$ mag. In the optical band the timescale is expected to be shorter, with a strongly suppressed peak brightness (e.g., 3 days and ~ -13 mag in *I*-band; 1 day and ~ -11 mag in *B*-band). Despite their low luminosity and fast timescale, kilonovae are of great interest as a detectable and isotropic counterpart to gravitational wave sources from the upcoming Advanced LIGO/Virgo experiments (e.g., Metzger & Berger 2012). At the same time, such transients should accompany short GRBs, if they can be discerned against the generally brighter and bluer afterglow emission.

In recent years there have been a few unsuccessful searches for a kilonova signature in short GRBs (Bloom et al. 2006; Perley et al. 2009; Kocevski et al. 2010), but these were focused in the optical band, which current models show to be strongly suppressed (Barnes & Kasen 2013). In this *Letter* we present the first detection of a kilonova, associated with GRB 130603B at $z = 0.356$. The results are based on a combination of early ground-based optical observations, coupled with optical and near-IR *HST* observations at a rest-frame time of about 1 week that reveal excess near-IR emission with an absolute magnitude and red optical/near-IR color that closely match the kilonova predictions. The presence of a kilonova provides strong evidence for compact object mergers as the progenitors of short GRBs, has crucial implications for the identification of electromagnetic counterparts to gravitational wave sources, and is indicative of compact object mergers as the primary site for the r-process.

2. OBSERVATIONS AND ANALYSIS

GRB 130603B was discovered with the *Swift* Burst Alert Telescope (BAT) on 2013 June 3.659 UT (Melandri et al. 2013), and was also detected with Konus-Wind (Golenetskii et al. 2013). The burst duration is $T_{90} = 0.18 \pm 0.02$ s (15 - 350 keV), with a fluence of $F_\gamma = (6.6 \pm 0.7) \times 10^{-6}$ erg cm⁻² (20 - 10⁴ keV), and a

¹ Harvard-Smithsonian Center for Astrophysics, 60 Garden Street, Cambridge, MA 02138, USA

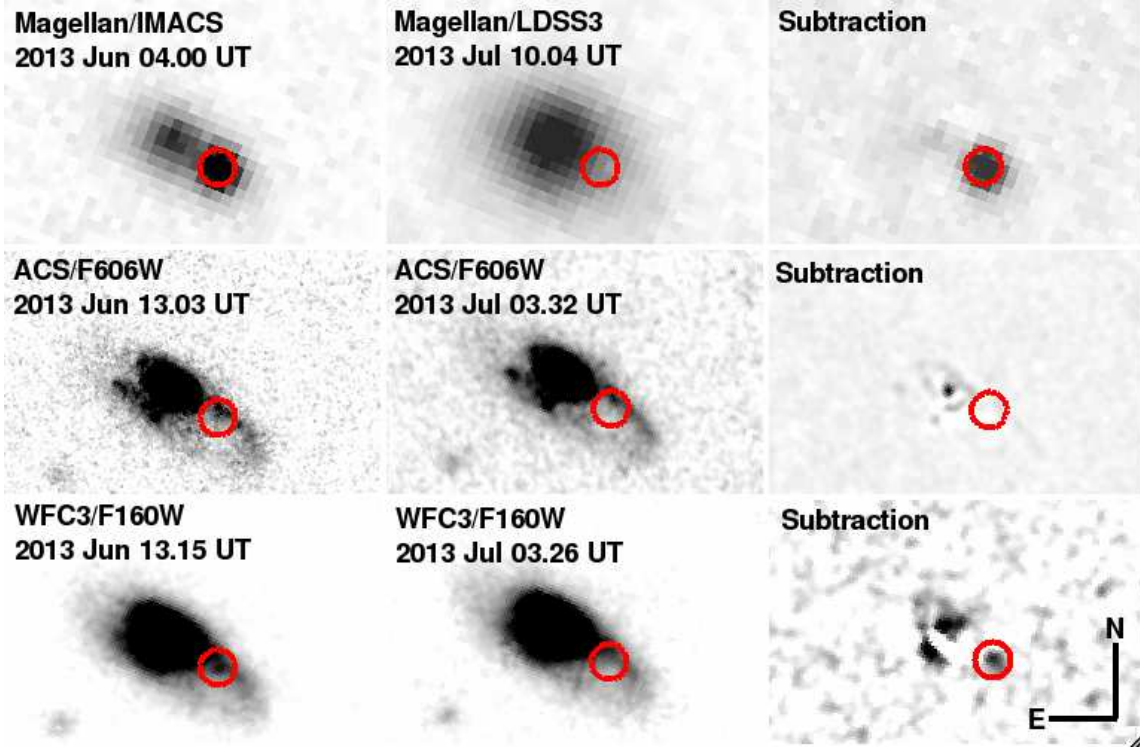


FIG. 1.— Magellan and *HST* observations of the afterglow and host galaxy of GRB 130603B. *Top*: Magellan/IMACS and LDSS3 *r*-band observations at 8.2 hr and 36.4 d, respectively, with the location of the afterglow marked. *Middle*: *HST*/ACS/F606W images. *Bottom*: *HST*/WFC3/F160W images. In all three rows the circle marks the location of GRB 130603B, with a radius of 10 times the rms of the astrometric match between the Magellan and *HST* images ($1\sigma \approx 34$ mas). A fading source coincident with the afterglow position is clearly visible in the WFC3/F160W image, with no corresponding counterpart in the ACS/F606W image.

peak energy of $E_p = 660 \pm 100$ keV (Melandri et al. 2013; Golenetskii et al. 2013). The spectral lags are 0.6 ± 0.7 ms (15–25 to 50–100 keV) and -2.5 ± 0.7 ms (25–50 to 100–350 keV), and there is no evidence for extended emission (Norris et al. 2013). The combination of these properties indicates that GRB 130603B is a short-hard burst. *Swift*/X-ray Telescope (XRT) observations commenced about 59 s after the burst and led to the identification of a fading source, with a UVOT-enhanced position of $RA=11^h28^m48.15^s$, $Dec=+17^\circ04'16.9''$ (1.4'' radius, 90% containment; Evans et al. 2013).

Ground-based observations starting at about 2.7 hr revealed a point source slightly offset from a galaxy visible in Sloan Digital Sky Survey (SDSS) images (Levan et al. 2013; de Ugarte Postigo et al. 2013; Foley et al. 2013; Sanchez-Ramírez et al. 2013; Cucchiara et al. 2013b). The point source subsequently faded away indicating that it is the afterglow of GRB 130603B (Cucchiara et al. 2013b). Spectroscopy of the host galaxy and afterglow revealed a common redshift of $z = 0.356$ (Thone et al. 2013; Foley et al. 2013; Sanchez-Ramírez et al. 2013; Cucchiara et al. 2013b; Xu et al. 2013). We obtained three sets of *r*-band observations of GRB 130603B with the Inamori Magellan Areal Camera and Spectrograph (IMACS) mounted on the Magellan/Baade 6.5-m telescope on June 4.00 ($t = 8.2$ hr) and 5.00 UT ($t = 32.2$ hr), and at late time with the Low Dispersion Survey Spectrograph (LDSS3) on the Magellan/Clay telescope on July 10.04 UT ($t = 36.4$ d; Fong et al. in preparation). Using digital image subtraction of the IMACS observations relative to the LDSS3 template image with the ISIS software package (Alard 2000) we detect the fading afterglow at a position of $RA=11^h28^m48.166^s$ and $Dec=+17^\circ04'18.03''$, with an uncertainty of 85 mas determined relative to SDSS. The centroid

uncertainty in the afterglow position is about 10 mas (Figure 1). The afterglow has $r = 21.56 \pm 0.02$ mag at 8.2 hr and $r \gtrsim 24.8$ mag (3σ) at 32.2 hr (all magnitudes are in the AB system and corrected for Galactic extinction).

Two epochs of *Hubble Space Telescope* Director’s Discretionary Time observations were undertaken on 2013 June 13.03 UT (ACS/F606W; 2216 s) and 13.15 UT (WFC3/F160W; 2612 s), as well as on 2013 July 3.29 UT (ACS/F606W; 2216 s) and 3.23 UT (WFC3/F160W; 2612 s). We retrieved the pre-processed images from the *HST* archive, and distortion-corrected and combined the individual exposures using the *astrodrizzle* package in PyRAF (Gonzaga et al. 2012). For the ACS image we used $\text{pixfrac} = 1.0$ and $\text{pixscale} = 0.05$ arcsec pixel $^{-1}$, while for the WFC3 image we used $\text{pixfrac} = 1.0$ and $\text{pixscale} = 0.0642$ arcsec pixel $^{-1}$, half of the native pixel scale. The final drizzled images, and subtractions of the two epochs with ISIS, are shown in Figure 1. To locate the afterglow position on the *HST* images, we perform relative astrometry between the IMACS and *HST* observations using 12 and 9 common sources for the WFC3/F160W and ACS/F606W images, respectively. The resulting rms uncertainty is 34 mas (1σ). The subtractions reveal a fading point source in the WFC3/F160W observations, coincident with the afterglow position, with no corresponding counterpart in the ACS/F606W observations (Figure 1).

To measure the brightness of the source we use point-spread-function (PSF) photometry with the standard PSF-fitting routines in the IRAF *daophot* package. We model the PSF in each image using 4 bright stars to a radius of $0.85''$, and apply the WFC3/F160W PSF to the point source in the subtracted image. Using the tabulated zeropoint, we obtain $m_{F160W} = 25.8 \pm 0.2$ mag. To determine the limit at the corresponding position in the ACS/F606W observation, we use the

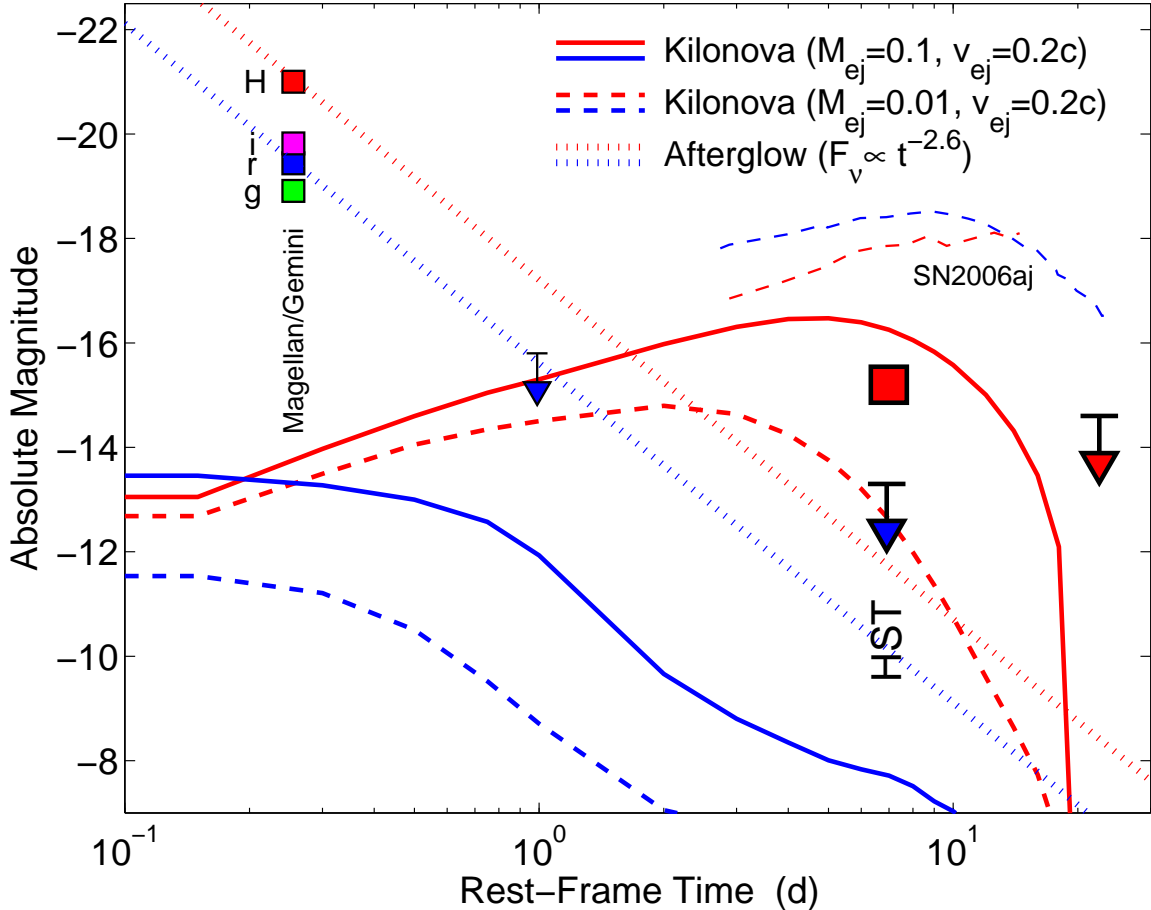


FIG. 2.— Absolute magnitude versus rest-frame time based on our ground-based observations from Magellan (§2), on Gemini data (Cucchiara et al. 2013b), and on our *HST* photometry (§2; blue: F606W; red: F160W). Also shown is an afterglow model with a single power law decline of $F_\nu \propto t^{-2.6}$, required by the ground-based observations. This model underpredicts the WFC3/F160W detection by about 3.5 mag. The thick solid and dashed lines are kilonova model light curves generated from the data in Barnes & Kasen (2013) and convolved with the response functions of the ACS/F606W and WFC3/F160W filters (solid: $M_{\text{ej}} = 0.1 M_\odot$; dashed: $M_{\text{ej}} = 0.01 M_\odot$). Finally, we also plot the light curves of GRB-SN 2006aj in the same filters (thin dashed; Ferrero et al. 2006; Kocevski et al. 2007), demonstrating the much fainter emission in GRB 130603B, and ruling out the presence of a Type Ic supernova (§3).

PSF to add fake sources of varying magnitudes at the afterglow position with the IRAF `addstar` routine, followed by subtraction with ISIS, leading to a 3σ limit of $m_{\text{F606W}} \gtrsim 27.7$ mag. Finally, to obtain a limit on the brightness of the source in the second epoch of WFC/F160W imaging we add fake sources of varying magnitudes at the source position and perform aperture photometry in a $0.15''$ radius aperture and a background annulus immediately surrounding the position of the source to account for the raised background level from the host galaxy. We find a 3σ limit of $m_{\text{F160W}} \gtrsim 26.4$ mag. We note that our detection of the near-IR source was subsequently confirmed by an independent analysis of the *HST* data (Tanvir et al. 2013). At the redshift of GRB 130603B, the resulting absolute magnitudes at 9.4 days are $M_H \approx -15.2$ mag and $M_V \gtrsim -13.3$ mag.

3. AN R-PROCESS KILONOVA

In principle, the simplest explanation for the near-IR emission detected in the *HST* data is the fading afterglow. To assess this possibility we note that our Magellan optical data at 8.2 and 32.2 hr require a minimum afterglow decline rate of $\alpha \lesssim -2.2$ ($F_\nu \propto t^\alpha$); *r*-band data from Gemini (Cucchiara et al. 2013b) require an even steeper decline of $\alpha \lesssim -2.6$. Similarly, the Gemini *gri*-band photometry at 8.4 hr indicates a spectral index of $\beta \approx -1.5$ (Cucchiara et al. 2013b), leading to inferred magnitudes in the *HST* filters of $m_{\text{F606W}} \approx 21.6$

mag and $m_{\text{F160W}} \approx 20.0$ mag (see Figure 2). Extrapolating these magnitudes with the observed decline rate to the time of the first *HST* observation we find expected values of $m_{\text{F606W}} \gtrsim 30.9$ mag and $m_{\text{F160W}} \gtrsim 29.3$ mag. While the inferred afterglow brightness in F606W is consistent with the observed upper limit, the expected F160W brightness is at least 3.5 mag fainter than observed. Moreover, the afterglow color at 8.4 hr is $m_{\text{F606W}} - m_{\text{F160W}} \approx 1.6$ mag, while at 9.4 days it is somewhat redder, $m_{\text{F606W}} - m_{\text{F160W}} \gtrsim 1.9$ mag, suggestive of a distinct emission component.

The excess near-IR flux at 9.4 days, with a redder color than the early afterglow, can be explained by emission from an *r*-process powered kilonova, subject to the large rest-frame optical opacities of *r*-process elements (Figure 2). In the models of Barnes & Kasen (2013), the expected rest-frame *B*–*J* color at a rest-frame time of 7 days (corresponding to the observed F606W–F160W color at 9.4 days) is exceedingly red, B – $J \approx 12$ mag, in agreement with the observed color. As shown in Figure 2, kilonova models with a fiducial velocity of $v_{\text{ej}} = 0.2c$ and ejecta masses of $M_{\text{ej}} = 0.01$ – $0.1 M_\odot$ bracket the observed near-IR brightness, and agree with the optical non-detection.

In Figure 3 we compare the observed F160W absolute magnitude to a grid of models from Barnes & Kasen (2013), calculated in terms of M_{ej} and v_{ej} . The grid is interpolated from the fiducial set of models in Barnes & Kasen (2013),

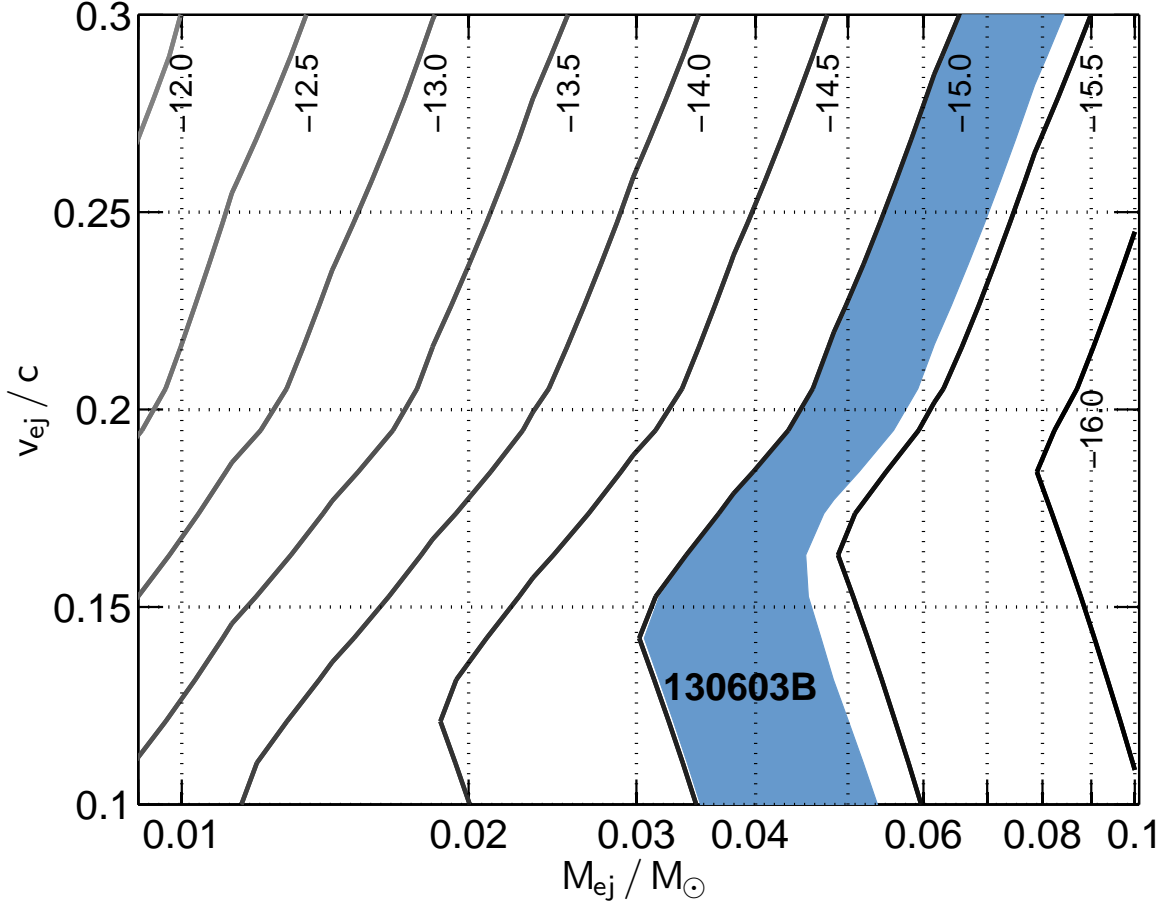


FIG. 3.— Contours of constant kilonova rest-frame J -band absolute magnitude at a rest-frame time of 6.9 days as a function of ejecta velocity and mass. The contours were calculated by convolving the kilonova models from Barnes & Kasen (2013), redshifted to $z = 0.356$, with the response functions of the ACS/F606W and WFC3/F160W filters. The solid region marks the F160W absolute magnitude of the kilonova associated with GRB 130603B. The observed brightness requires an ejecta mass of $M_{\text{ej}} \approx 0.03 - 0.08 M_{\odot}$ for $v_{\text{ej}} \approx 0.1 - 0.3c$.

with $M_{\text{ej}} = 10^{-3}, 10^{-2}, 10^{-1} M_{\odot}$ and $v_{\text{ej}} = 0.1c, 0.2c, 0.3c$. We then redshift the models, convolve them with the response function of the WFC3/F160W filter, and compare the results to contours of fixed absolute magnitude to determine the model parameters. We find that for GRB 130603B the observed absolute magnitude requires $M_{\text{ej}} = 0.03 - 0.08 M_{\odot}$ for $v_{\text{ej}} = 0.1 - 0.3c$. Thus, a kilonova can account for the observed emission, and the observations place a scale of $\sim \text{few} \times 10^{-2} M_{\odot}$ for the ejected mass. We note that using other recent kilonova models (Rosswog et al. 2013; Tanaka & Hotokezaka 2011) leads to similar results. The inferred ejecta mass agrees with the results of merger simulations, which predict $M_{\text{ej}} \sim (0.5 - 5) \times 10^{-2} M_{\odot}$ (depending on the mass ratio of the binary constituents; Goriely et al. 2011; Piran et al. 2013).

Finally, we stress that the faint emission detected in the *HST* data rules out the presence of an associated Type Ic supernova. In particular, at a rest-frame time of 7 days the GRB-SN 1998bw had $M_B \approx -18.2$ mag (Galama et al. 1998) at least 4.9 mag brighter than GRB 130603B. Similarly, GRB-SN 2003lw had $M_J \approx -17.8$ mag (Gal-Yam et al. 2004), about 2.6 mag brighter than GRB 130603B. Even the relatively dim GRB-SN 2006aj has $M_B \approx -18.4$ mag (Ferrero et al. 2006) and $M_J \approx -17.9$ mag (Kocevski et al. 2007), $\gtrsim 5.1$ mag and 2.7 mag brighter than GRB 130603B, respectively (Figure 2). The normal Type Ic SN 2002ap had $M_B \approx -16.5$ mag and $M_J \approx -16.3$ mag on this timescale (Yoshii et al. 2003), also well in excess of the observed brightness for

GRB 130603B. Indeed, only SN 2008D had comparable observed absolute magnitudes, $M_B \approx -13.4$ mag and $M_J \approx -15.6$ mag (Soderberg et al. 2008; Modjaz et al. 2009), but this supernova was heavily reddened, with $E(B - V) \approx 0.6$ mag (Soderberg et al. 2008). We therefore conclude that the short GRB 130603B was not accompanied by a Type Ic supernova typical of long GRBs, or even a non-GRB Type Ib/c supernova, indicating that its progenitor was not a massive star.

4. CONCLUSIONS

Using *HST* optical and near-IR observations we identify a fading near-IR source with $M_H \approx -15.2$ mag and $V - H \gtrsim 1.9$ mag at 9.4 days post-burst. The observed emission is at least 25 times brighter than expected from an extrapolation of the fading afterglow, as measured from our Magellan observations and from multi-band Gemini data (Cucchiara et al. 2013b). A kilonova model with $M_{\text{ej}} \approx 0.03 - 0.08 M_{\odot}$ (for $v_{\text{ej}} = 0.1 - 0.3c$) provides a good match to both the absolute magnitude in the near-IR and the red optical/near-IR color, making GRB 130603B the first short burst with evidence for r-process rich ejecta, a clear signature of compact object mergers. The inferred ejecta mass is in good agreement with the results of numerical simulations for a wide range of compact object binaries (Goriely et al. 2011; Piran et al. 2013). In addition, the faint optical/near-IR emission rules out an association with a Type Ic supernova typical of those that accompany long GRBs, or even non-GRB Type Ib/c supernovae, demonstrating that the progenitor of GRB 130603B was not a mas-

sive star.

In addition to providing strong evidence for compact object mergers as the progenitors of short GRBs, the detection of a kilonova has additional key implications. First, the inferred ejecta mass coupled with the (albeit poorly known) rate of compact object mergers, suggests that such mergers are likely to be the primary site for the r-process (Lattimer & Schramm 1976; Lattimer et al. 1977; Korobkin et al. 2013). Second, the observed H -band brightness and the inferred ejecta mass indicate that for a typical NS-NS merger detected at the Advanced LIGO/Virgo range of 200 Mpc, the optical I -band magnitude will be $\sim 23.5-24.5$ in the first week, while J -band will reach a peak of ~ 21.5 mag. Given the current lack of wide-field near-IR imagers capable of covering the typical Advanced LIGO/Virgo localization regions ($\sim 10^2$ deg 2) to this depth, this indicates that searches in the reddest optical filters (izy) with wide-field imagers on large telescopes (e.g., Pan-STARRS, DECam, Subaru, LSST) will provide the most

promising route to the electromagnetic counterparts of gravitational wave sources. GRB 130603B is likely to become the benchmark for these searches.

We thank Ryan Foley and Paul Harding for obtaining the Magellan observations, and Dan Kasen for sharing his kilonova models. The Berger GRB group at Harvard is supported by the National Science Foundation under Grant AST-1107973. Based on observations made with the NASA/ESA Hubble Space Telescope, obtained from the Data Archive at the Space Telescope Science Institute, which is operated by the Association of Universities for Research in Astronomy, Inc., under NASA contract NAS 5-26555. These observations are associated with program #13497. This paper includes data gathered with the 6.5 meter Magellan Telescopes located at Las Campanas Observatory, Chile.

Facilities: Magellan, HST

REFERENCES

- Alard, C. 2000, *A&AS*, 144, 363
 Barnes, J., & Kasen, D. 2013, arXiv:1303.5787
 Berger, E. 2010, *ApJ*, 722, 1946
 Berger, E. 2011, *New Astronomy Reviews*, 55, 1
 Berger, E., Cenko, S. B., Fox, D. B., & Cucchiara, A. 2009, *ApJ*, 704, 877
 Berger, E., et al. 2005, *Nature*, 438, 988
 Bloom, J. S., et al. 2006, *ApJ*, 638, 354
 Cucchiara, A., Prochaska, J. X., Perley, D. A., Cenko, S. B., Werk, J., Cao, Y., Bloom, J. S., & Cobb, B. E. 2013b, arXiv:1306.2028
 de Ugarte Postigo, A., Malesani, D., Xu, D., Jakobsson, P., Datson, J., RSalinas, R., Augusteijn, T., & Martinez-Osorio, Y. 2013, *GRB Coordinates Network*, 14743, 1
 Eichler, D., Livio, M., Piran, T., & Schramm, D. N. 1989, *Nature*, 340, 126
 Evans, P. A., Goad, M., Osborne, J., & Beardmore, A. 2013, *GRB Coordinates Network*, 14739, 1
 Ferrero, P., et al. 2006, *A&A*, 457, 857
 Foley, R. J., Chornock, R., Fong, W., & Berger, E. 2013, *GRB Coordinates Network*, 14745, 1
 Fong, W., & Berger, E. 2013, arXiv:1307.0819
 Fong, W., et al. 2013, *ApJ*, 769, 56
 Fong, W., et al. 2011, *ApJ*, 730, 26
 Fong, W., Berger, E., & Fox, D. B. 2010, *ApJ*, 708, 9
 Gal-Yam, A., et al. 2004, *ApJ*, 609, L59
 Galama, T. J., et al. 1998, *Nature*, 395, 670
 Gehrels, N., et al. 2005, *Nature*, 437, 851
 Golenetskii, S., et al. 2013, *GRB Coordinates Network*, 14771, 1
 Goriely, S., Bauswein, A., & Janka, H.-T. 2011, *ApJ*, 738, L32
 Hjorth, J., et al. 2005a, *ApJ*, 630, L117
 Hjorth, J., et al. 2005b, *Nature*, 437, 859
 Kocevski, D., et al. 2007, *ApJ*, 663, 1180
 Kocevski, D., et al. 2010, *MNRAS*, 404, 963
 Korobkin, O., Rosswog, S., Arcones, A., & Winteler, C. 2012, *MNRAS*, 426, 1940
 Lattimer, J. M., & Schramm, D. N. 1976, *ApJ*, 210, 549
 Lattimer, J. M., Mackie, F., Ravenhall, D. G., & Schramm, D. N. 1977, *ApJ*, 213, 225
 Levan, A. J., Tanvir, N., Wiersema, K., Hartoog, O., Kolbe, K., Mendez, J., & Kupfer, T. 2013, *GRB Coordinates Network*, 14742, 1
 Li, L.-X., & Paczyński, B. 1998, *ApJ*, 507, L59
 Melandri, A., et al. 2013, *GRB Coordinates Network*, 14735, 1
 Metzger, B. D., & Berger, E. 2012, *ApJ*, 746, 48
 Metzger, B. D., et al. 2010, *MNRAS*, 406, 2650
 Modjaz, M., et al. 2009, *ApJ*, 702, 226
 Narayan, R., Paczynski, B., & Piran, T. 1992, *ApJ*, 395, L83
 Norris, J., Gehrels, N., Barthelmy, S., & Sakamoto, T. 2013, *GRB Coordinates Network*, 14746, 1
 Paczynski, B. 1991, *Acta Astronomica*, 41, 257
 Perley, D. A., et al. 2009, *ApJ*, 696, 1871
 Piran, T., Nakar, E., & Rosswog, S. 2013, *MNRAS*, 430, 2121
 Rosswog, S., Korobkin, O., Arcones, A., & Thielemann, F.-K. 2013, arXiv:1307.2939
 Sanchez-Ramírez, R., et al. 2013, *GRB Coordinates Network*, 14747, 1
 Soderberg, A. M., et al. 2006, *ApJ*, 650, 261
 Soderberg, A. M., et al. 2008, *Nature*, 453, 469
 Tanaka, M., & Hotokezaka, K. 2013, arXiv:1306.3742
 Tanvir, N. R., et al. 2013, arXiv:1306.4971
 Thone, C. C., de Ugarte Postigo, A., Gorosabel, J., Tanvir, N., & Fynbo, J. 2013, *GRB Coordinates Network*, 14744, 1
 Xu, D., et al. 2013, *GRB Coordinates Network*, 14757, 1
 Yoshii, Y., et al. 2003, *ApJ*, 592, 467
 Zheng, Z., Flynn, C., Gould, A., Bahcall, J. N., & Salim, S. 2001, *ApJ*, 555, 393